EARTHQUAKE ENGINEERING AND STRUCTURAL DYNAMICS
Earthquake Engng Struct. Dyn. (2010)
Published online in Wiley Online Library (wileyonlinelibrary.com). DOI: 10.1002/eqe.1087

Extension of the CSM-FEMA440 to plan-asymmetric real building structures

Carlos Bhatt*, † and R. Bento

Instituto Superior Técnico, Technical University of Lisbon, Lisbon, Portugal

SUMMARY

The capacity spectrum method (CSM) has established itself as one of the most used Nonlinear Static Procedures for the seismic assessment of structures, since its introduction in 1975, when it was first presented by Freeman. More recently, this procedure was implemented in the ATC40 guidelines and lately improved in the FEMA-440 report. The first step of work addressed by this paper relates to the comparison between the two features of the CSM. In the second part, an extension of the FEMA-440CSM version is proposed for plan-asymmetric real RC building structures. The case studies under analysis are the SPEAR building—an irregular 3D structure representing typical old three-storey buildings in the Mediterranean region, from the early 1970s—and two real Turkish buildings with five and eight storeys. The CSM-ATC40, the CSM-FEMA440 and the proposed extended CSM-FEMA440 method are applied and the results obtained duly compared with nonlinear dynamic *timehistory* analyses. For the latter, semi-artificial ground motions are used to define the seismic action. Copyright © 2010 John Wiley & Sons, Ltd.

Received 2 June 2010; Revised 24 October 2010; Accepted 26 October 2010

KEY WORDS: pushover analysis; capacity spectrum method; ATC40; FEMA-440; torsion; plan-asymmetric real building structures

1. INTRODUCTION

The nonlinear static procedures constitute nowadays a very practical tool to perform nonlinear structural analyses. In fact, they represent significantly less time consuming than nonlinear dynamic analysis. The latter are obviously more accurate in terms of results, although the increasing number of updating formulations of the different available NSPs drive them to very good performances, namely, in regular buildings and planar frames. These results are supported by extensive verifications, such as [1, 2].

In 1975, Freeman and collaborators presented for the first time the innovative capacity spectrum method—the so-called CSM [3]. Since then, this method has gained considerable popularity among pushover users and the ATC40 guidelines [4] included it as the recommended nonlinear static procedure to be used. Later, the FEMA440 report [5] came out with an updated version of the method increasing the precision of its results.

Despite the fact that these methods represent a very good approach of the inelastic range of planar structures, the behaviour of 3D plan-asymmetric buildings still cannot be totally reproduced by the majority of the existing NSPs. These irregular structures represent the usual case in real life, so accurate pushover methods are needed to be implemented in designing codes and taking into account the torsion effects. Recent attempts have been made to develop pushover formulations

*Correspondence to: Carlos Bhatt, Instituto Superior Técnico, Technical University of Lisbon, Lisbon, Portugal.
†E-mail: cbhatt@civil.ist.utl.pt

capable of predicting the torsional response of irregular structures. A breakthrough of innovative methods has occurred, such as [6–8].

In this paper, three realistic RC plan-asymmetric buildings with different number of storeys, subjected to bi-axial excitation are scrutinized. The action applied in the nonlinear dynamic analyses is constituted by two sets of semi-artificial ground motions fitted to each building's correspondent Eurocode8's response spectrum. As a first step of this work, a comparison between the CSM with the features recommended in the ATC40 and in the FEMA440 is made. Afterwards, an extension of the CSM-FEMA440 procedure to overcome the torsional problem in plan-asymmetric buildings is proposed. This proposal was based on the results presented by Fajfar *et al.* [7] and advocates that torsional amplification can be computed through the combination of a linear elastic analysis with a pushover analysis. The precision of this new procedure is illustrated with the normalized top displacements of the buildings under analysis.

2. CASE STUDIES

2.1. Three-storey SPEAR building

The SPEAR building represents typical existing three-storey buildings in the Mediterranean region following Greece's concrete design code in force between 1954 and 1995. This structure was designed only for gravity loads based on the construction practice applied in the early 1970s that included the use of smooth rebars. It was tested in full-scale under pseudo-dynamic conditions, and subjected to bi-direction seismic loading, at JRC Ispra within the European SPEAR project framework. Plan and elevation views are shown in Figure 1, while further details on the structure and its pseudo-dynamic testing can be found in [9, 10].

The building is plan-asymmetric in both X and Y directions, but it is regular in elevation (Figure 1). Eight of the nine existing columns have a square cross-section of $250 \times 250\,\text{mm}^2$. The column C6 has a rectangular section of $250 \times 750\,\text{mm}^2$, with the higher dimension oriented along the Y direction implying a 'weak direction' along the X-axis. The column C6 and the presence of a balcony on the east side of the structure are the major causes for the in-plan irregularity, shifting the centre of mass (CM) away from the centre of stiffness (CR), which is very close to the central column (C3), thus causing the eccentricity to be larger in the Y direction.

2.2. Five-storey Turkish building

The five-storey Turkish structure is a real Turkish-reinforced concrete five-storey building that experienced the 1999 Golcuk earthquake without any damage. The building is asymmetric along the X-axis (Figure 2(a)) and all the floors have the same height (Figure 2(b)). The structure presents

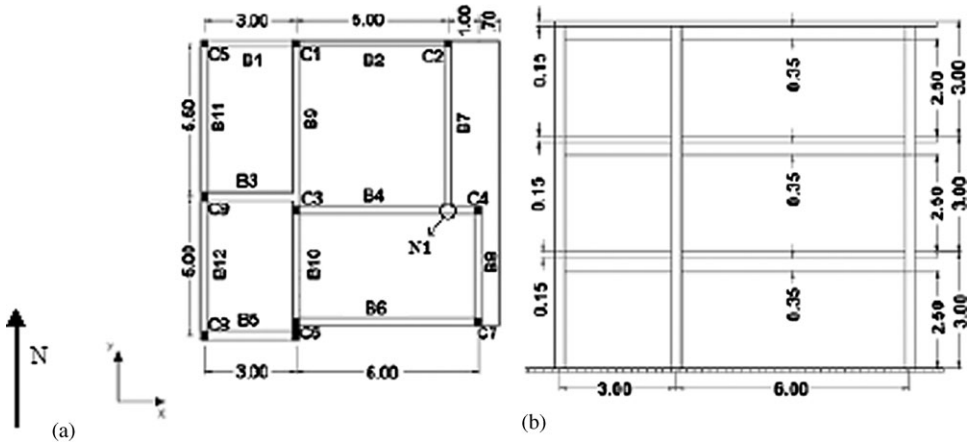

Figure 1. Three-storey building: (a) plan view and (b) lateral view (units in metres).

DOI: 10.1002/eqe

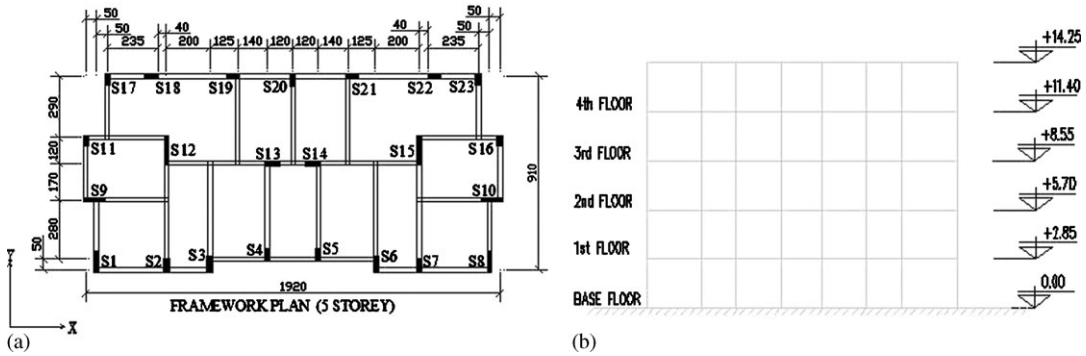

Figure 2. Five-storey building: (a) plan view (cm) and (b) lateral view (m).

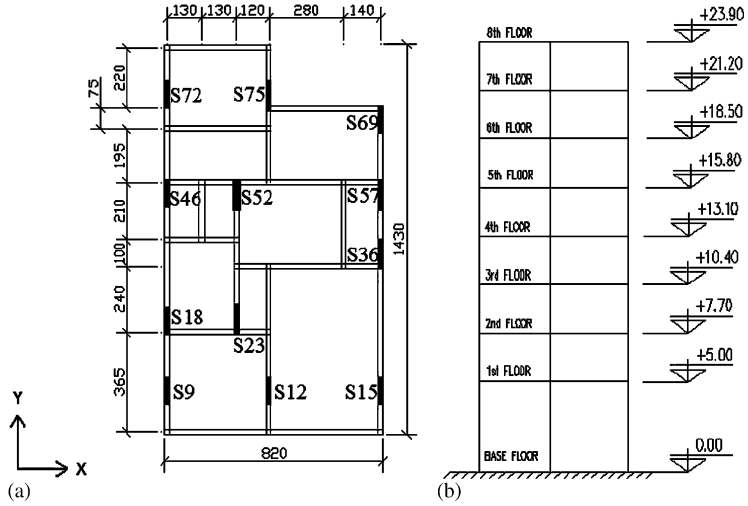

Figure 3. Eight-storey building: (a) plan view (cm) and (b) lateral view (m).

beams framing into beams, leading to possible weak connections in the structure. There are also walls and elongated columns, as shown in Figure 2.

Column sections maintain geometrical and reinforcement features constant along the building's height. The slabs are 0.10 and 0.12 m thick. The beam sections are mainly $0.20 \times 0.50\,\mathrm{m}^2$ except the two located in the centre of the building that are $0.20 \times 0.60\,\mathrm{m}^2$. The stirrups have 20 cm spacing both for beams and columns. For more details on the building's characteristics, see [11].

2.3. *Eight-storey Turkish building*

The eight-storey structure is also a real Turkish-reinforced concrete building. It is a plan-asymmetric structure in both X- and Y-axis (Figure 3(a)). The first storey is 5.00 m height and the upper floors have the same 2.70 m height (Figure 3(b)). Along the lines of what happened in the previous buildings, there are beams framing into beams, walls and elongated columns with the higher dimension always along the Y direction (Figure 3). For this reason, the structure will be stiffer and resistant along the Y direction. The column sections maintain the same geometrical features along the height, except the column S52 that varies from $1.1 \times 0.3\,\mathrm{m}^2$ (on the first floor) to $0.8 \times 0.3\,\mathrm{m}^2$ (on the last floor). The height of this section is reduced in 0.1 m every two storeys. The beam sections are mainly $0.20 \times 0.50\,\mathrm{m}^2$ except the two located in the centre of the building along the X direction that are $0.30 \times 0.50\,\mathrm{m}^2$ and $0.25 \times 0.50\,\mathrm{m}^2$, respectively. The slabs are 0.12 m thick.

DOI: 10.1002/eqe

3. NUMERICAL MODELLING

The analysis software adopted in this work was SeismoStruct [12], a freely downloadable fibre element-based finite element program.

The 3D models representing the buildings under analysis were built using space frames assuming the centreline dimensions. The beams that have other beams being framed were subdivided to have a node at the beam being framed in order to respect the model cinematic compatibility. This type of modelling did not create any particular numerical issue. The members' inelasticity was modelled through the use of fibre element models. Each fibre was characterized by the respective material relationship.

The column–beam end connections were not modelled with rigid offsets; however, elongated columns were modelled as wall elements due to their larger dimension.

Hysteretic damping was already implicitly included in the nonlinear fibre model formulation of the inelastic frame elements.

In order to take into account for possible non-hysteretic sources of damping, a tangent stiffness-proportional damping was used. For the SPEAR building, a value of 2% was used , according to the experimental results at ISPRA, and for the Turkish buildings a 5% value was considered.

The concrete was represented by a uniaxial model that follows the constitutive relationship proposed by Mander *et al.* [13] and the cyclic rules proposed by Martinez-Rueda and Elnashai [14]. The confinement effects provided by the lateral transverse reinforcement are taken into account through the rules proposed by Mander *et al.* [13] whereby constant confining pressure is assumed throughout the entire stress–strain range. A compressive strength of 25 MPa was considered for the SPEAR building and 16.7 MPa for the Turkish buildings.

The constitutive model used for the steel was the one proposed by Menegotto and Pinto [15] coupled with the isotropic hardening rules proposed by Filippou *et al.* [16]. The average yield strength of 360 MPa was assumed for the SPEAR building and 371 MPa for the Turkish buildings.

The Nodal Constraints with Penalty Functions option were taken to model the rigid diaphragm effect in the Turkish buildings. The penalty function exponent used was 10^7. To model this characteristic of the slab in the SPEAR building it was used the Rigid Diaphragm with Lagrange multipliers modelling strategy. This option resulted from the calibration of the analytical model with the experimental results.

The comparisons between the analytical results and the experimental tests for the SPEAR building can be found in Bento *et al.* [8].

4. SEISMIC ASSESSMENT—PARAMETRIC STUDY

4.1. Seismic action

For the three-storey SPEAR building, seven bi-directional semi-artificial ground motion records from the SPEAR project were considered (Table I). These records had been fitted to the EC8 [17] elastic design spectrum (Type 1 soil C).

Table I. Ground motion records considered.

Earthquake name	Station name
Imperial Valley 1979	Bonds Corner
Loma Prieta 1989	Capitola
Kalamata 1986	Kalamata-Prefecture
Montenegro 1979	Herceg Novi
Friuli 1976	Tolmezzo
Montenegro 1979	Ulcinj2
Imperial Valley 1940	El Centro Array #9

DOI: 10.1002/eqe

Table II. Records used in this study.

Earthquake name	Year	ClstD (km)	Earthquake magnitude	Site classification Campbell's geocode	Mechanism based on rake angle
Tabas, Iran	1978	13.94	7.35	Firm rock	Reverse
Whittier Narrows-01	1987	40.61	5.99	Very firm soil	Reverse-oblique
Northridge-01	1994	37.19	6.69	Firm rock	Reverse

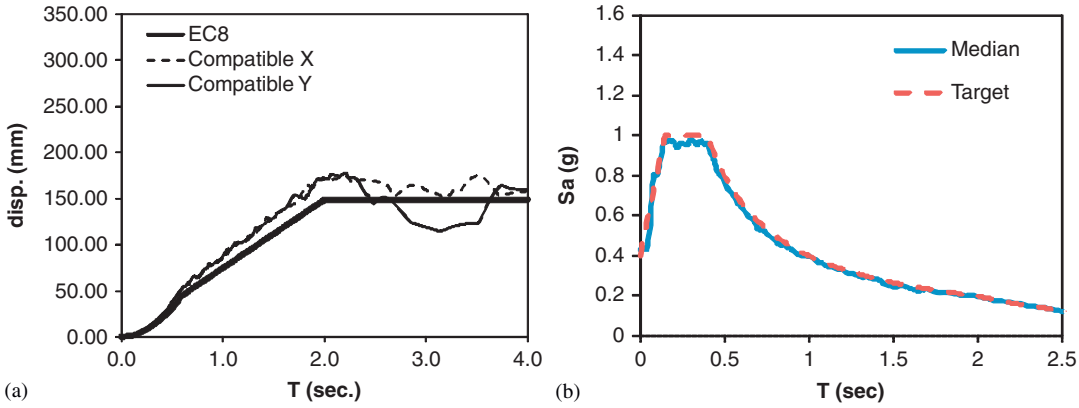

Figure 4. (a) Displacement spectra defined for SPEAR building ($0.2g$) and (b) acceleration spectra defined for Turkish buildings ($0.4g$).

For the Turkish buildings, three bi-directional semi-artificial ground motion records were considered. These three records are real ones (Table II) and were taken from the PEER's database website [18]. They were fitted to the Eurocode8 elastic design spectrum (with the Turkish code features—Type 1 soil A) using the software RSPMatch2005 [19].

In order to assess the sensitivity of the NSPs to different intensities, the ground motions were scaled for different intensity levels. Therefore, the accelerograms were scaled for peak ground accelerations of 0.05, 0.1, 0.2 and $0.3g$ for the three-storey building and 0.1, 0.2, 0.4, 0.6 and $0.8g$ for the Turkish buildings.

The correspondent response spectrum of each record was computed. Afterwards, the median of these spectra was obtained for each set. These median spectra were used to compute the target displacements in the NSPs and they are represented in Figure 4(a) and (b) as defined for the three-storey SPEAR building and for the Turkish buildings, respectively. In these figures the EC8's response spectra with which the accelerograms were matched are also represented.

4.2. Structural analyses carried out

In the pushover analysis, lateral forces were applied to the structure in the form of a modal load pattern. The loads were applied independently in the two horizontal positive/negative directions, resulting in four analyses. For each one, the target displacement was computed with the larger value in each direction being chosen. The results were combined in the two directions using the SRSS combination.

For the nonlinear dynamic analysis of the three-storey SPEAR building the aforementioned seven bi-directional semi-artificial ground motion records were employed in four different configurations: $X+Y+$, $X+Y-$, $X-Y-$, $X-Y+$.

For the nonlinear dynamic analysis of the Turkish buildings, the above-mentioned three bi-directional semi-artificial ground motion records were employed. Each record was applied twice in the structure changing the direction of the components, resulting in six models, each one with five intensity levels for the five-storey building and three intensity levels for the eight-storey buildings.

DOI: 10.1002/eqe

The results in terms of displacement patterns, interstorey drifts, chord rotations, top displacements, base shear and normalized top displacements in the two directions were calculated and compared for all seismic intensity levels and for all nonlinear static and dynamic analyses.

5. A COMPARISON BETWEEN THE CSM-ATC40 AND THE CSM-FEMA440

In this section, the CSM-ATC40 and the CSM-FEMA440 features are briefly described, emphasizing the differences between the two procedures. Both methods involve a pushover analysis with a modal load pattern. The structural capacity curve expressed in terms of roof displacement and base shear is then converted into a single degree of freedom (SDOF) curve in terms of displacements and accelerations through the application of a transformation factor. The demand spectrum, with which the capacity curve will be intersected, must have an ADRS format (acceleration–displacement response spectrum). This demand spectrum is reduced using a reduction factor (usually depending on the effective damping) and then intersected with the capacity curve in order to find a first performance point (Figure 5). For this point a new effective damping can be computed and hence a new reduction factor can be applied. The new intersection between the capacity curve and the new reduced spectrum leads to a new performance point. If the target displacement calculated is within a tolerable range, then the performance point can be obtained. Otherwise, the iterative process continues until one finds convergence. The difference between the ATC40 guidelines and the FEMA440 report lies on the estimation of damping and on the computation of the response spectrum's reduction factor.

The specificities of both methods in computing the effective damping and the reduction factor are explained as follows.

5.1. ATC40

The Procedure A of the ATC40 guidelines to calculate the target displacements was used in this work.

5.1.1. Estimation of damping and reduction in the response spectrum. When a structure subjected to a ground motion gets into the inelastic range the damping associated is a combination of a viscous damping and a hysteretic damping. This guideline defines an equivalent viscous damping to represent this combination and it can be calculated using Equation (1).

This expression applied to the existing reinforced concrete buildings, which are not typically ductile structures, overestimates realistic damping levels. To overcome this problem, ATC40 introduces the concept of effective viscous damping that can be obtained multiplying the equivalent

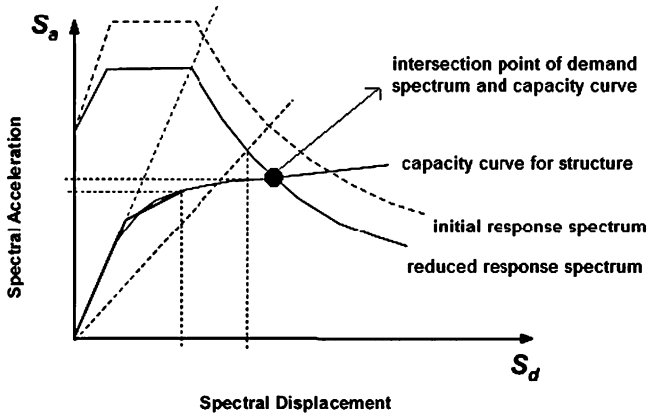

Figure 5. General CSM procedure to compute the target displacement (modified from [5]).

DOI: 10.1002/eqe

damping by a modification factor k (Equation (2)).

$$\beta_{eq} = \beta_0 + 5 \tag{1}$$

$$\beta_{eff} = k\beta_0 + 5 \tag{2}$$

where β_{eq} is the equivalent viscous damping, β_{eff} is the effective viscous damping, k is the damping modification factor, β_0 is the hysteretic damping represented as equivalent viscous damping, 5–5% viscous damping inherent in the structure (assumed to be constant).

The hysteretic damping represented as the equivalent viscous damping can be calculated using the following equation:

$$\beta_0 = \frac{63.7(a_y d_{pi} - d_y a_{pi})}{a_{pi} d_{pi}} \tag{3}$$

where a_{pi} and d_{pi} correspond to a trial performance point, for instance, the intersection between the capacity curve and the demand spectrum. The capacity curve should be bilinearized in this trial point, considering a post-yield stiffness. a_y and d_y correspond to this bilinear curve yielding point.

Hence, the effective damping can be written as following:

$$\beta_{eff} = \frac{63.7k(a_y d_{pi} - d_y a_{pi})}{a_{pi} d_{pi}} + 5 \tag{4}$$

The damping modification factor k measures the extent to which the actual building hysteresis is well represented by the parallelogram illustrated in Figure 6, either initially or after degradation.

The k-factor depends on the structural behaviour of the building, which depends on the seismic resisting system quality and the duration of ground shaking. ATC40 defines three categories of structural behaviour. In this work, Type B characterizes the structural behaviour of the buildings and it represents a moderate reduction in the area of the parallelogram (Figure 6).

Table III indicates the β_0 and k values corresponding to the structural behaviour type B.

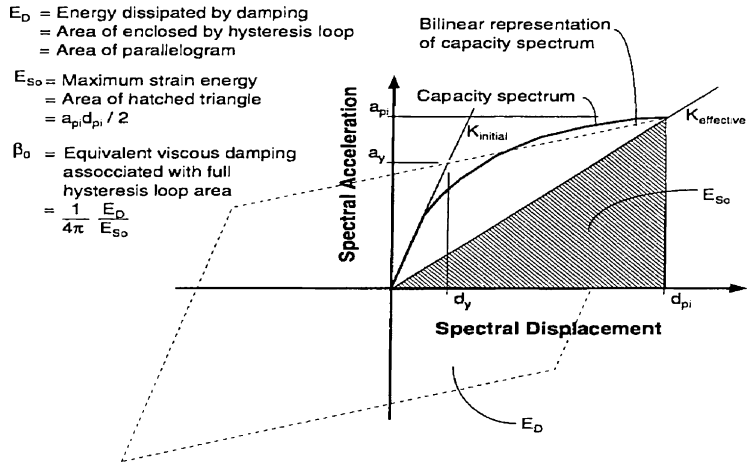

Figure 6. Hysteresis parallelogram [4].

Table III. Modification factor k.

Structural behaviour type	β_0 (%)	k
Type B	$\leqslant 25$	0.67
	>25	$0.845 - \frac{0.446(a_y d_{pi} - d_y a_{pi})}{a_{pi} d_{pi}}$

DOI: 10.1002/eqe

5.1.2. Numerical derivation of spectral reduction. The spectral reduction factors are calculated as shown in the following equations:

$$SR_A = \frac{3.21 - 0.68\ln(\beta_{\text{eff}})}{2.12} = \frac{3.21 - 0.68\ln\left[\dfrac{63.7\,k(a_y d_{pi} - d_y a_{pi})}{a_{pi} d_{pi}} + 5\right]}{2.12} \geqslant 0.44 \tag{5}$$

$$SR_V = \frac{2.31 - 0.41\ln(\beta_{\text{eff}})}{1.65} = \frac{2.31 - 0.41\ln\left[\dfrac{63.7k(a_y d_{pi} - d_y a_{pi})}{a_{pi} d_{pi}} + 5\right]}{1.65} \geqslant 0.56 \tag{6}$$

One should multiply the response spectrum by these factors in order to reduce it.

5.2. FEMA440

In this endeavour the FEMA440's Procedure B—Intersection with MADRS (modified acceleration–displacement response spectrum)—is used to calculate the target displacement.

5.2.1. Effective damping. The formulas herein presented apply to any capacity curve, independent of hysteretic model type or post-elastic stiffness value (named as alpha) used.

The effective damping is calculated using Equation (7), (8) or (9) depending on the structure's level of ductility μ

$$\text{For } \mu < 4.0: \quad \beta_{\text{eff}} = 4.9(\mu - 1)^2 - 1.1(\mu - 1)^3 + \beta_0 \tag{7}$$

$$\text{For } 4.0 \leqslant \mu \leqslant 6.5: \quad \beta_{\text{eff}} = 14.0 + 0.32(\mu - 1) + \beta_0 \tag{8}$$

$$\text{For } \mu > 6.5: \quad \beta_{\text{eff}} = 19\left[\frac{0.64(\mu - 1) - 1}{[0.64(\mu - 1)]^2}\right]\left(\frac{T_{\text{eff}}}{T_0}\right)^2 + \beta_0 \tag{9}$$

where μ is the ductility, β_0 is the initial damping (5%-concrete buildings), T_0 is the fundamental period in the direction under consideration, T_{eff} is the effective period.

5.2.2. Effective period. Once again, the following equations apply to any capacity spectrum independent of the hysteretic model type or post-elastic stiffness value. The effective period depends on the ductility level and is calculated using the following equations:

$$\text{For } \mu < 4.0: \quad T_{\text{eff}} = \{0.20(\mu - 1)^2 - 0.038(\mu - 1)^3 + 1\}T_0 \tag{10}$$

$$\text{For } 4.0 \leqslant \mu \leqslant 6.5: \quad T_{\text{eff}} = [0.28 + 0.13(\mu - 1) + 1]T_0 \tag{11}$$

$$\text{For } \mu > 6.5: \quad T_{\text{eff}} = \left\{0.89\left[\sqrt{\frac{(\mu - 1)}{1 + 0.05(\mu - 2)}} - 1\right] + 1\right\} T_0 \tag{12}$$

5.2.3. Spectral reduction factor for effective damping. The spectral reduction factor is a function of the effective damping and is named damping coefficient, $B(\beta_{\text{eff}})$, and it is calculated using Equation (14). It is used to adjust spectral acceleration ordinates as shown in the following equation:

$$(S_a)_\beta = \frac{(S_a)_{5\%}}{B(\beta_{\text{eff}})} \tag{13}$$

$$B = \frac{4}{5.6 - \ln\beta_{\text{eff}}(\text{in}\%)} \tag{14}$$

DOI: 10.1002/eqe

5.2.4. Modified acceleration–displacement response spectrum (MADRS). After reducing the initial ADRS by using the $B(\beta_{\text{eff}})$ factor, as described in Equation (13), one should multiply the acceleration ordinates (i.e. not the displacement ordinates) of the newly reduced ADRS by the modification factor, M. This factor is determined using the calculated effective period, T_{eff}, as shown in Equations (15) and (16), in order to compute the MADRS

$$M = \left(\frac{T_{\text{eff}}}{T_{\text{s}}}\right)^2 = \left(\frac{T_{\text{eff}}}{T_0}\right)^2 \left(\frac{T_0}{T_{\text{s}}}\right)^2 \tag{15}$$

$$\frac{T_{\text{s}}}{T_0} = \sqrt{\frac{\mu}{1+\alpha(\mu-1)}} \tag{16}$$

where α is the post-elastic stiffness and μ the ductility, calculated as follows:

$$\alpha = \frac{\left(\frac{a_{pi}-a_y}{d_{pi}-d_y}\right)}{\left(\frac{a_y}{d_y}\right)} \tag{17}$$

$$\mu = \frac{d_{pi}}{d_y} \tag{18}$$

The MADRS should be intersected with the capacity curve in an iterative procedure, in order to compute the performance point.

5.3. Analysis results

The comparison of results obtained with the two methods will be presented in this subsection. The *timehistory* median results are identified in each plot as TH.

In Figures 7 and 8, the lateral displacement profiles for all the buildings under analysis are compared with the CSM-ATC40, the CSM-FEMA440 and the *timehistory* analysis.

Based on Figures 7 and 8 it can be concluded that the CSM-FEMA440 presents very good results for the columns located near the CM of the buildings, when compared with the nonlinear dynamic analysis. For the columns located on the extremities of the buildings, the method slightly underestimates the response (see Figure 7(c)). The CSM-ATC40 gives invariantly under conservative results. These conclusions can be taken for both the X and Y directions, for all ground shaking intensities and for all the buildings analysed.

The interstorey drift profiles are presented next and compared for different intensity levels.

From Figure 9(b) and (c) one can observe that the CSM-FEMA440 usually leads to better estimations of the interstorey drifts profiles than the CSM-ATC40 for the columns located near the

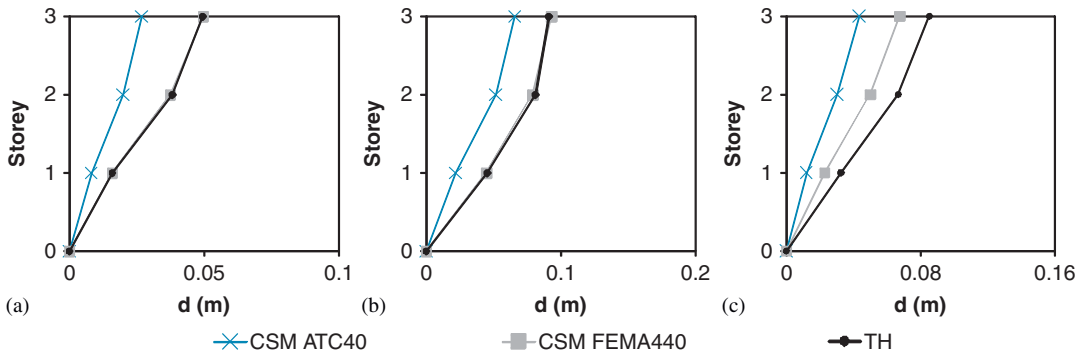

Figure 7. Three storey: (a) X-direction column C3, $0.1g$; (b) X-direction column C3, $0.2g$; and (c) Y-direction column C8, $0.2g$.

DOI: 10.1002/eqe

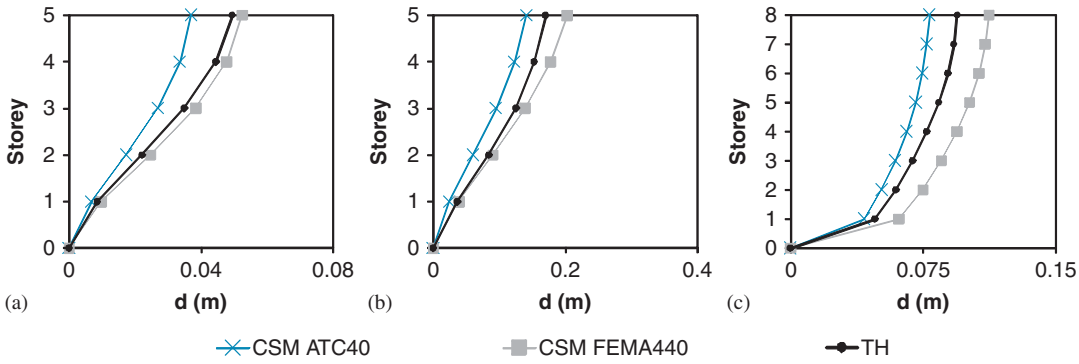

Figure 8. (a) Five storey X-direction column S13, 0.2g; (b) five storey Y-direction column S14, 0.6g; and (c) eight storey X-direction column S23, 0.2g.

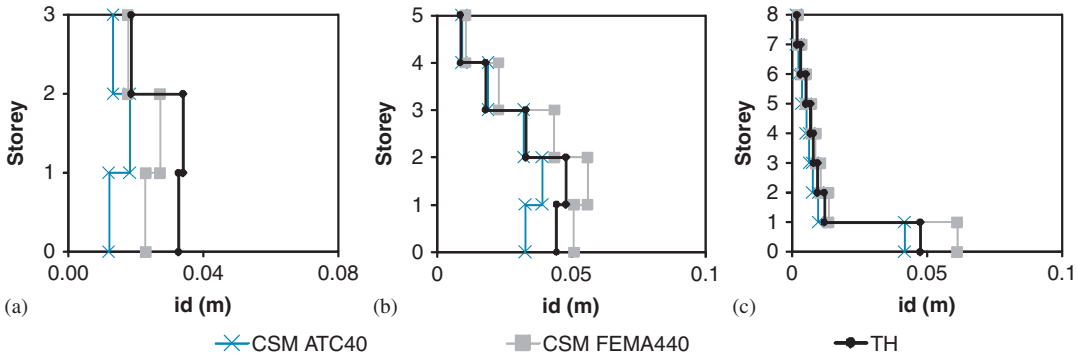

Figure 9. (a) Three storey Y-direction column C8, 0.2g; (b) five storey X-direction column S14, 0.6g; and (c) eight storey X-direction column S23, 0.2g.

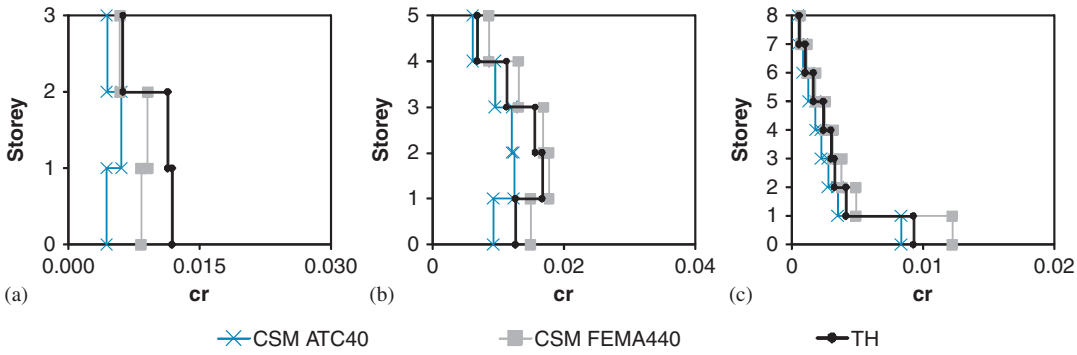

Figure 10. (a) Three storey Y-direction column C8, 0.2g; (b) five storey Y-direction column S1 0.6g; and (c) eight storey X-direction column S52, 0.2g.

CM of the buildings. For the columns located on the periphery of the buildings the method slightly underestimates the response (Figure 9(a)). The CSM-ATC40 leads once again to underestimated results, except in the three upper storeys of the five-storey building for column S14 in the X direction for a 0.6g seismic intensity. For this case, the CSM-FEMA440 slightly overestimates the interstorey drifts profile.

The chord rotation profiles are now presented for the different buildings and for the methods under comparison in Figure 10. From Figure 10 it is possible to conclude that the CSM-FEMA440 estimates in a very accurate way the chord rotations in columns near the centre of mass (Figure 10(b)

DOI: 10.1002/eqe

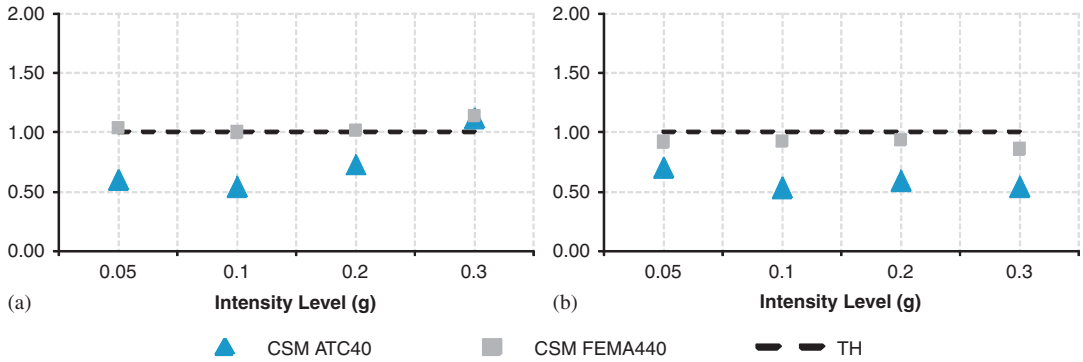

Figure 11. Three-storey building CM top displacement: (a) X direction and (b) Y direction.

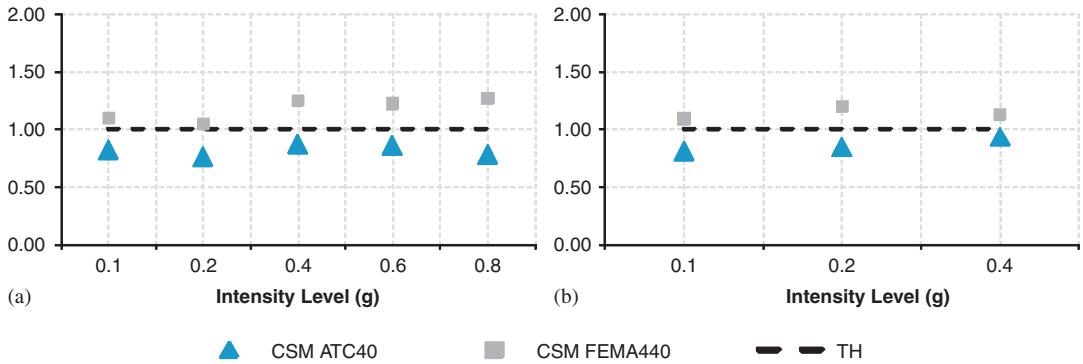

Figure 12. CM top displacement: (a) five-storey building Y direction and (b) eight-storey building X direction.

and (c)). For columns located in the periphery of the buildings (Figure 10(a)), the method cannot perfectly reproduce the structural seismic response. One can observe that the CSM-ATC40 generally underestimates the chord rotations profiles for all the buildings analysed.

The CSM-FEMA440 can capture in a very good manner the soft storey on the first floor of the eight-storey building, whereas the CSM-ATC40 slightly underestimates this effect (Figures 8(c), 9(c) and 10(c)).

In order to get a quick overview of how the different NSPs perform, ratios of the values obtained with the latter for different response parameters and the corresponding median estimates coming from the nonlinear dynamic analysis (Equation (19)) are computed. Ideally one would desire such ratios to tend to unity

$$\text{Top displacement ratio} = \frac{\text{NSP's top displacement}}{\text{Time history median top displacement}} \tag{19}$$

Similar ratios were computed for other response quantities, such as interstorey drift, base shears, all in both X and Y directions, leading to similar observations and conclusions.

Figures 11 and 12 illustrate target displacements computed for the three buildings in both directions for different intensity levels.

From Figure 11, it is clear that target displacements computed using CSM-FEMA440 perfectly match the *timehistory* in both directions and for the different intensity levels. The exception occurs in the Y direction for $0.3g$, corresponding to a very high level of inelasticity, where the response is slightly under conservative. The target displacements computed with the CSM-ATC40 are nonconservative in both directions and for the different intensity levels, except in the X direction for $0.3g$ where the response matches quite well the *timehistory* results.

DOI: 10.1002/eqe

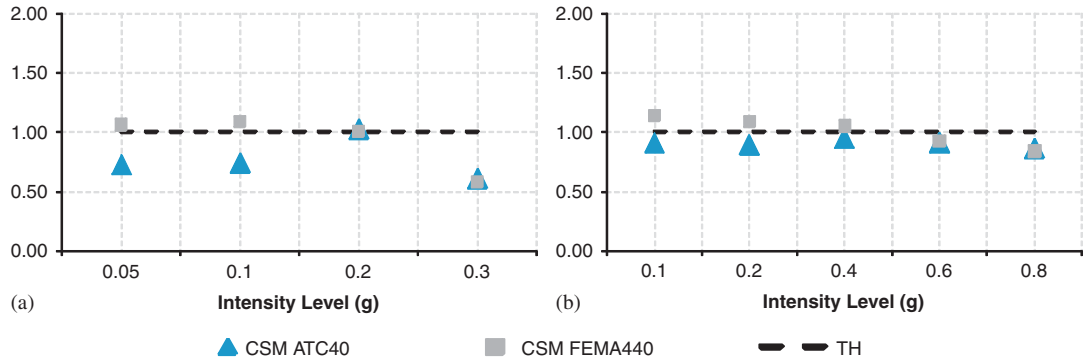

Figure 13. Base shear: (a) three-storey building X direction and (b) five-storey building X direction.

Table IV. Three-storey building—effective damping values.

	Three-storey building: 2% equivalent viscous damping			
	X ($T = 0.617$ s)		Y ($T = 0.441$ s)	
Intensity level (g)	ATC40 (%)	FEMA440 (%)	ATC40 (%)	FEMA440 (%)
0.05	6.4	2.1	5.7	2.1
0.1	12.0	2.2	10.1	2.1
0.2	13.6	5.8	10.6	3.2
0.3	25.8	15.9	15.8	5.8

For the five-storey building and for the eight-storey building (Figure 12) one can conclude that the CSM-FEMA440 leads to conservative target displacements for increasing intensity levels, while the CSM-ATC40 underestimates the response.

The base shear indexes of the buildings under analysis are plotted in Figure 13 for increasing levels of seismic intensity.

From Figure 13 it is possible to identify a trend on the base shear index computed using the CSM-FEMA440 for the three buildings under study. For increasing seismic intensities, mainly when the building goes through high inelastic ranges, the base shear index tends to decrease in all buildings. For these high levels of inelasticity the method slightly underestimates the response. When the buildings behave elastically and inelastically (but not with a high level of inelasticity) the CSM-FEMA440 is able to estimate correctly the base shear response. On the other hand, the CSM-ATC40 generally underestimates the base shear response in all buildings, for all intensity levels and in both directions. The exception occurs in the three-storey building, in the X direction for $0.2g$ where the method estimates correctly the base shear.

5.4. Discussion

The results aforepresented show that the CSM-FEMA440 estimates in a very accurate way the response of the CM and the response of the columns located near this node, where the torsional effect is not very marked, through all the seismic intensities analysed. On the contrary, the CSM-ATC40 leads to a generally underestimated response of these elements. These differences can be justified due to different estimations of effective period and damping computed by these two methods. This fact is easily observed in the elastic range, where the effective damping calculated with these procedures should be equal to the equivalent viscous damping considered for each building in the nonlinear dynamic analysis. In the case of the three-storey building, a 2% viscous damping was used in the nonlinear *timehistory*. One can verify in Table IV that the ATC40 overestimates the effective damping in both directions to seismic intensities of 0.05 and $0.1g$, for which the building remains elastic. On the other hand, the FEMA440 seems to estimate the

DOI: 10.1002/eqe

Table V. Five-storey building—effective damping values.

	Five-storey building: 5% equivalent viscous damping			
	X ($T=0.617$ s)		Y ($T=0.593$ s)	
Intensity level (g)	ATC40 (%)	FEMA440 (%)	ATC40 (%)	FEMA440 (%)
0.1	12.8	5.2	13.2	5.4
0.2	13.8	5.3	13.6	5.3
0.4	17.3	6.7	16.6	6.4
0.6	23.0	10.9	22.2	10.0
0.8	25.5	18.9	24.3	15.6

damping in a very accurate way. In the five-storey and eight-storey buildings the equivalent viscous damping used in the *timehistory* analysis was 5%. The five-storey building remains elastic for 0.1 and 0.2g and the eight storey for 0.1g. It is important to mention that this last case behaves elastically in the Y direction through all the seismic intensities studied. In both five-storey, see Table V, and eight-storey buildings the ATC40 overestimates once again the effective damping, while the FEMA440 seems to reproduce it in a very good fashion. The overestimation of the effective damping in the elastic range, compared with the equivalent viscous damping used in the *timehistory*, by the ATC40 for the three buildings under analysis justifies the underestimated results obtained by this method. On the other hand, the innovative methods to compute the effective damping by the FEMA440 explain the good results obtained with this method in the CM and in columns near this node.

All the buildings analysed in this study in both X and Y directions have short/medium periods (less than 2 s), see Tables IV and V. The differences in the results of the two NSPs for these short/medium-period buildings in the elastic range can be justified by the high sensitivity of the μ value in the CSM procedure to small errors in estimating the period and damping ratio. In fact, the elastic response spectrum tends to be very jagged in the short-period range. Therefore, the calculation of the elastic SDOF system becomes very sensitive to errors in the vibration period and damping ratios. In the elastic range, the values of μ used in the ATC40 and in the FEMA440 to compute the effective period and the effective damping may become larger than one (in the elastic range the μ should theoretically be equal to one). Thus, the two NSPs lead to different responses for short/medium-period buildings [20]. This fact also justifies the differences in the results obtained with the ATC40 and FEMA440 procedures in the elastic range. The elastic response spectrum in the long-period range tends to be smooth; therefore, the errors in the vibration period and damping ratio do not affect so drastically the target displacement estimation, and consequently the μ of the long-period buildings in the elastic range. Probably, the results of the two methods would not be so different for long-period structures behaving elastically.

In the inelastic range the underestimated results obtained with the ATC40 procedure can also be justified by its overestimation of the effective damping. The three-storey building behaves inelastically for 0.2 and 0.3g, the five-storey building for 0.4, 0.6 and 0.8g and the eight-storey building goes through the inelastic range for 0.2 and 0.4g only in the X direction. From Tables IV and V one can see that the values of effective damping calculated with the ATC40 are much higher than the ones obtained with FEMA440 for these seismic intensities. The buildings under analysis have poor ductility so the high values of damping obtained with the ATC40 in the inelastic range seem quite unrealistic. This fact confirms the trend previously observed in the elastic range. The results obtained with FEMA440 are close to the *timehistory* leading to the conclusion that the effective damping calculated with this method is in fact more realistic.

In the columns located on the extremities of the buildings (away from the CM), the results obtained with the CSM-FEMA440 are closer to the *timehistory* than the ones obtained with the CSM-ATC40, although they seem to be not so exact as the ones obtained to the CM. This happens because none of the algorithms contemplate any special feature in order to capture the torsional motion induced by the earthquake. In order to overcome this shortcoming, an extension of the

DOI: 10.1002/eqe

CSM-FEMA440 for plan-asymmetric buildings is presented in the following section. Since this method leads to better results than the ATC40, the authors will neglect it in the next comparisons.

The buildings analysed in this study have poor ductility, so the conclusions outlined herein can only be drawn for this type of structures. For high-ductility buildings, further studies must be developed in order to outline definitive conclusions.

6. AN EXTENSION OF THE CSM-FEMA440 FOR PLAN-ASYMMETRIC BUILDINGS

The big issue when dealing with plan-asymmetric buildings, which usually leads to a less accurate performance of the currently used nonlinear static procedures, is torsion. To overcome this problem, an extension of the aforementioned CSM-FEMA440 is herein proposed for non-symmetric in-plan buildings. This method was chosen to be extended because it led to better results than its counterpart recommended in ATC40, as observed in Section 5. This proposal is based on the results of extensive studies developed by Fajfar *et al.* [7]. The outcomes outlined by this team were taken to extend the N2 method to the case of buildings with such kind of irregularities. It was concluded that in the majority of buildings an upper bound of the torsional amplifications can be determined by a linear dynamic (response spectrum) analysis also in the inelastic range.

An extended version of the CSM-FEMA440 is thus proposed in this paper. It takes into account the contribution of a pushover analysis, with the calculation of the target displacement based on the FEMA440 recommendations, and the contribution of a linear response spectrum analysis (RSA) in order to capture the amplification due to torsion. The reduction in demand due to torsion is neglected. The entire procedure can be summarized in the following steps:

(1) Perform pushover analyses with positive and negative sign for each X and Y direction of a 3D numerical model. Compute the target displacement—displacement demand at the CM at roof level—for each direction as the larger value of the + and − sign pushover. For this calculation use the CSM-FEMA440 recommendations described in Section 5.
(2) Perform a linear modal RSA in two X and Y directions combining the results according to the SRSS rule.
(3) Determine the torsional correction factors. This factor is computed using the ratio between the normalized roof displacements obtained by the elastic RSA and by the pushover analysis. The normalized roof displacement is obtained by normalizing the displacement value at a specific location with respect to those of the CM. If the normalized roof displacement obtained from the elastic RSA is smaller than 1.0, one should consider 1.0 to avoid any favourable torsional effect (reduction of displacements) given by the elastic analysis.
(4) Multiply the quantity under study for a certain location by the correction factor calculated for that location.

6.1. Assessment of the new procedure

The proposed procedure is applied to the three-, five- and eight-storey buildings under analysis. In order to evaluate the torsional response of the buildings the results in terms of normalized top displacements are presented. This measure is obtained by normalizing the edge displacement values with respect to those of the CM.

In each of the subsequent plots, the RSA represents the results of the elastic RSA and the TH the median results of the *timehistory* analysis. In Figure 14(a), very good agreement between the extended CSM-FEMA440 and the *timehistory* results for the three-storey building in the X direction is observed for an intensity level of $0.1g$. The original CSM-FEMA440 presents a good match with the *timehistory* in the column C8, while in column C2 this method underestimates significantly the response. The torsional amplification in column C2 is correctly captured by the extended CSM-FEMA440. The RSA leads to underestimated results in column C8 when compared with the *timehistory*, but it matches quite perfectly the response of column C2. Note that in this last column the results of the RSA are the same of the ones obtained with the extended CSM-FEMA440.

DOI: 10.1002/eqe

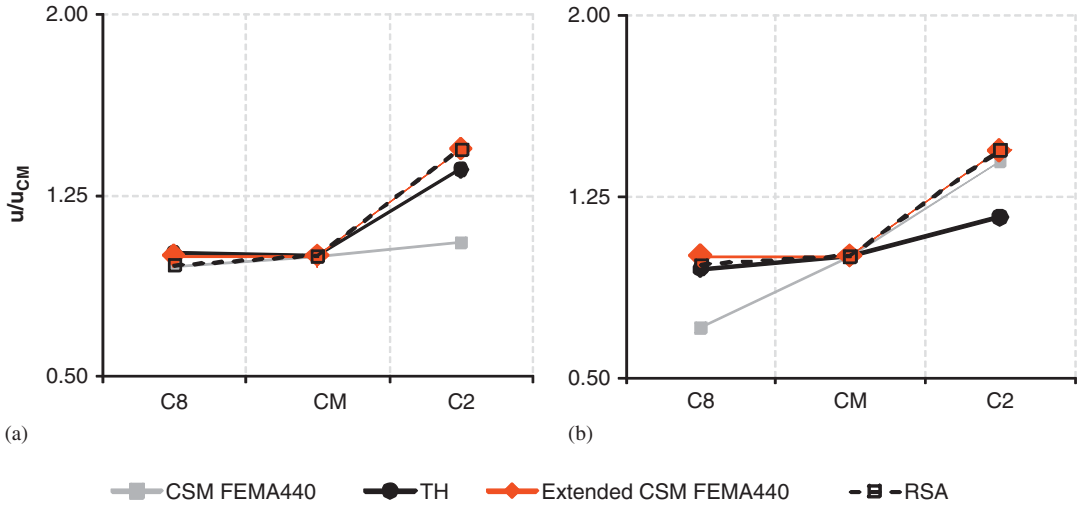

Figure 14. Three-storey building X direction: (a) $0.1g$ and (b) $0.3g$.

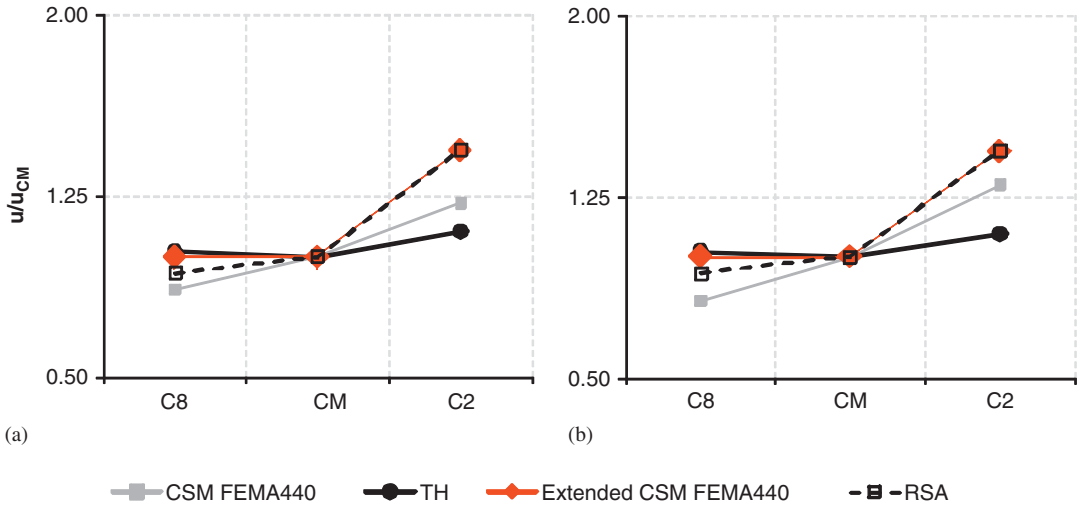

Figure 15. Three-storey building Y direction: (a) $0.2g$ and (b) $0.3g$.

In Figure 14(b), for $0.3g$ still in the X direction, one can observe a very good performance of the proposed method for the column C8. In fact, the results match perfectly with the *timehistory* ones. For this column the original method presents under conservative results. For column C2 both original and extended CSM-FEMA440 presents conservative results. The RSA reproduces in a very good way the behaviour of column C8, and it overestimates it in column C2. The RSA results in column C2 correspond to the ones of the extended CSM-FEMA440.

In the Y direction, for the three-storey building, for both 0.2 and $0.3g$ (Figure 15) the response of the column C8 is perfectly reproduced by the proposed procedure, while the original method underestimates the results. In fact, the unrealistic favourable effect of torsion given by the original CSM-FEMA440 in this side of the building is not considered by the extended procedure. For both intensity levels, the results for the column C2 are overestimated by both methods. The RSA underestimates the results in column C8 for both intensities, but it matches the response of the extended CSM-FEMA440 in column C2.

In Figure 16 is represented the response of the five-storey building in the X direction for 0.1 and $0.2g$. Based on the results obtained one can conclude that for column S1 the proposed procedure

DOI: 10.1002/eqe

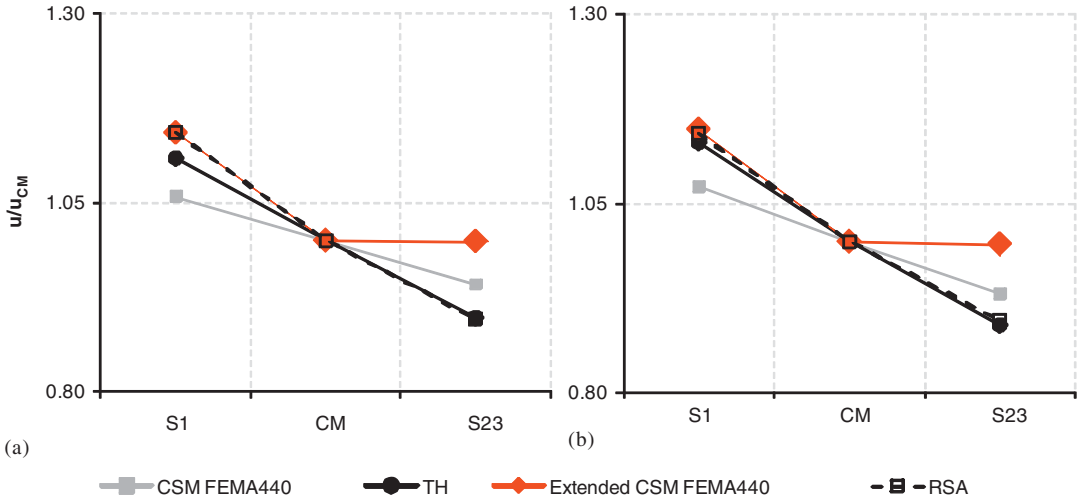

Figure 16. Five-storey building X direction: (a) $0.1g$ and (b) $0.2g$.

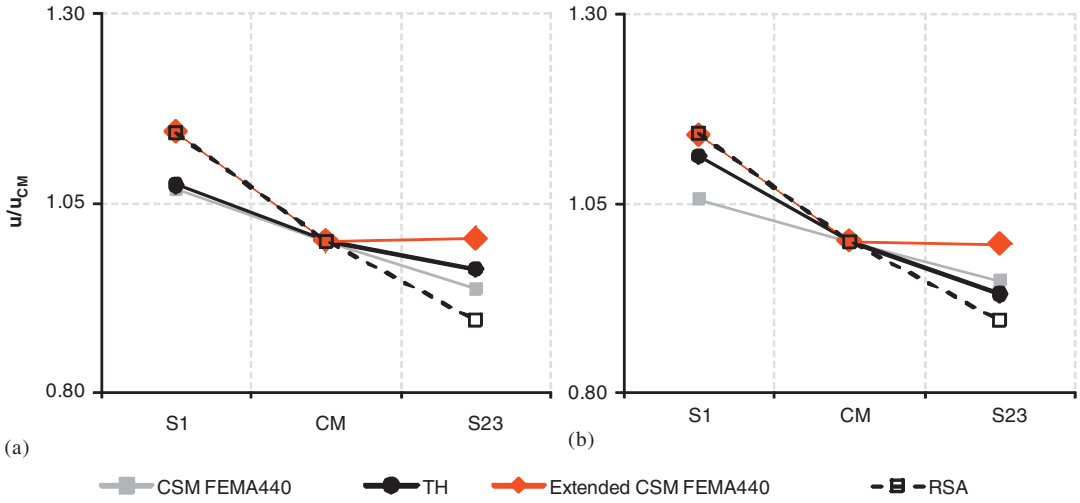

Figure 17. Five-storey building X direction: (a) $0.4g$ and (b) $0.6g$.

reproduces perfectly the realistic response, while the original procedure leads to underestimated results. In column S23 both methods lead to conservative results. The RSA reproduces in a very accurate way the *timehistory* results in both sides of the building for both intensity levels.

From the plots of Figure 17 it is observed that for column S1 the proposed method gives conservative results for $0.4g$ and a good match for $0.6g$.

For the same column, the original procedure leads to a good response for $0.4g$ and to under conservative results for $0.6g$. In column S23, the extended CSM-FEMA440 gives always conservative results, while the original method leads to an under conservative response for $0.4g$ and to a good match for $0.6g$. The RSA considerably underestimates the response of column S23 for both intensities and it matches the extended CSM-FEMA440 results in column S1.

For the X direction but for $0.8g$ (Figure 18(a)), once again the extended method herein proposed leads to conservative results in column S1 and to a very good match in column S23. The original method matches perfectly the response of column S1 but underestimates the results for column S23. The response of column S23 is once again underestimated by the RSA for this intensity level.

DOI: 10.1002/eqe

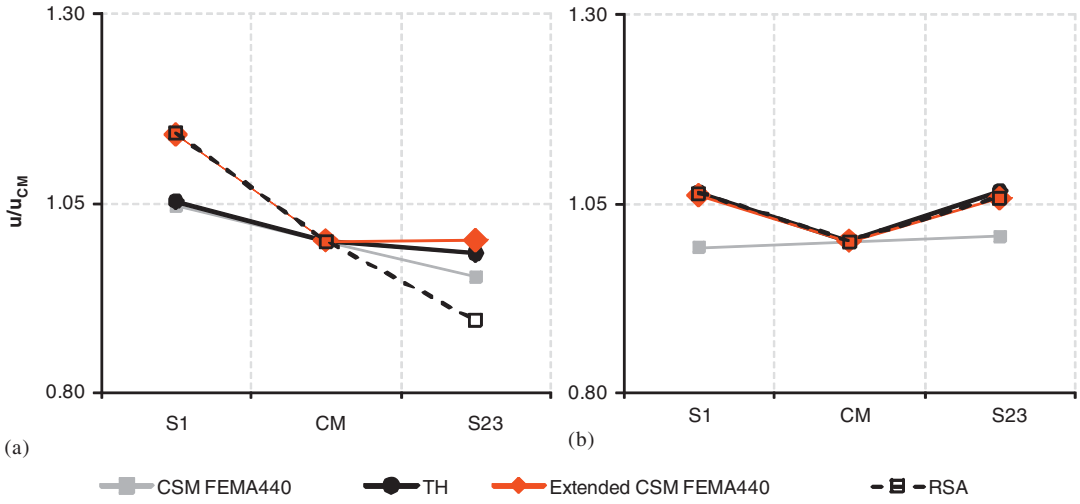

Figure 18. Five-storey building: (a) X direction $0.8g$ and (b) Y direction $0.8g$.

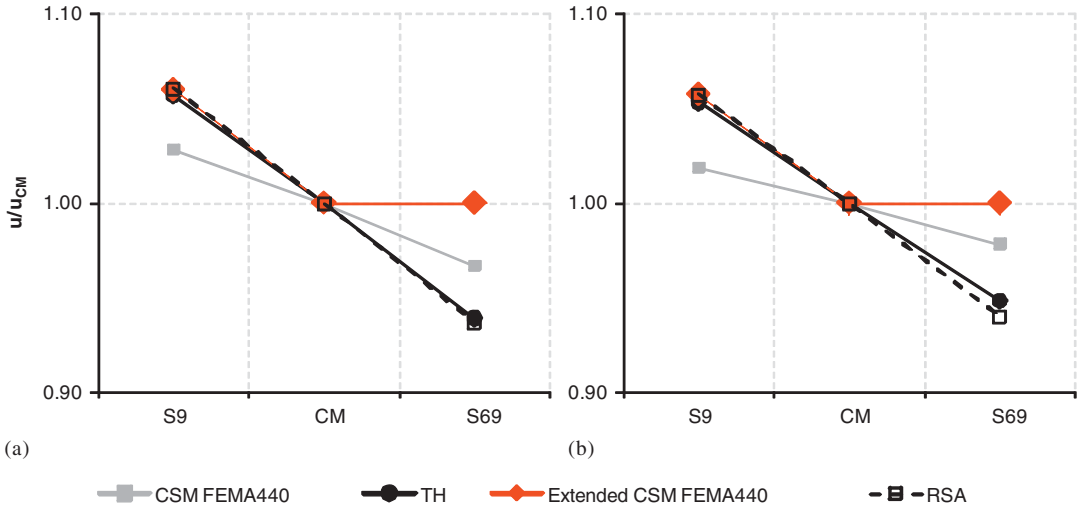

Figure 19. Eight-storey building X direction: (a) $0.1g$ and (b) $0.2g$.

In the Y direction for $0.8g$ (Figure 18(b)), the torsional motion of the building is perfectly reproduced by the extended CSM-FEMA440 and by the RSA. The original method underestimates the response in both sides of the building.

In the eight-storey building the extended CSM-FEMA440 captures perfectly the response of the column S9 for both 0.1 and $0.2g$ in the X direction (Figure 19). For this column the original procedure leads to nonconservative results. The response of column S69 is overestimated by both methods. The same conclusions can be drawn for the X direction for $0.4g$ (Figure 20(a)). The RSA reproduces perfectly the *timehistory* results in the X direction for all the intensity levels analysed.

In the Y direction for $0.4g$ (Figure 20(b)), both methods reproduce quite well the torsional motion of the building, except the original procedure that slightly underestimates the response of the column S9. The RSA underestimates the results in column S9 in the Y direction for $0.4g$, but it matches the extended CSM-FEMA440 in column S69.

DOI: 10.1002/eqe

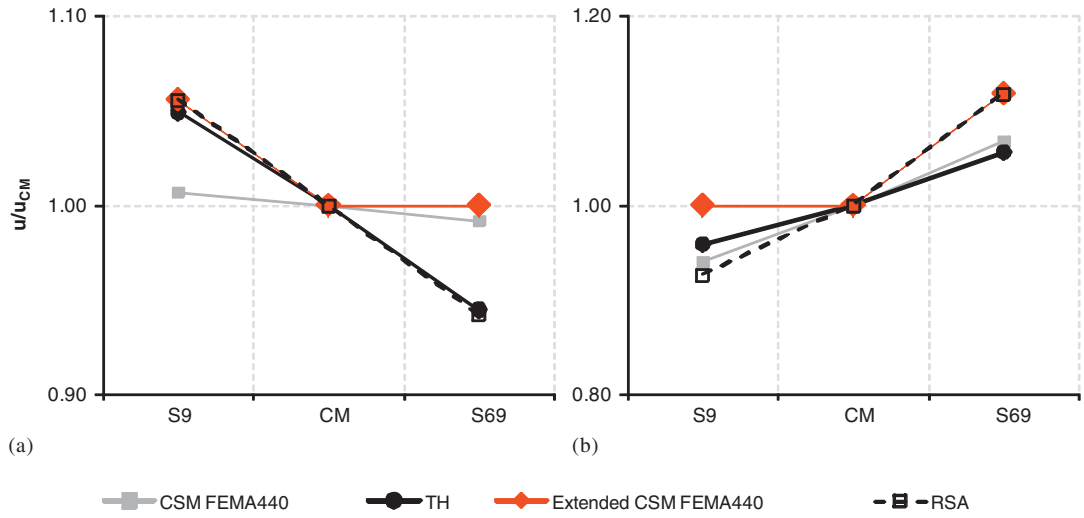

Figure 20. Eight-storey building: (a) X direction $0.4g$ and (b) Y direction $0.4g$.

6.2. *Discussion*

From the presented results one can conclude that the extended CSM-FEMA440 herein proposed captures in a more accurate fashion the torsional motion of the studied buildings for all seismic intensities than the original CSM-FEMA440 procedure.

From the plots aforepresented it is observed that the extended CSM-FEMA440 perfectly reproduces the torsional amplification in all buildings through all the seismic intensities in both directions. This happens because the method uses a correction factor based on an RSA which also leads to very good estimations of the torsional amplifications, as shown in the plots. The original CSM-FEMA440 generally underestimates the torsional amplification in the buildings.

The plots also show that both RSA and the original CSM-FEMA440 consider the torsional deamplification. In some cases these methods led to underestimated results. On the other hand, the extended CSM-FEMA440 does not consider any positive effect due to torsion, as explained before in the description of the procedure, leading in some cases to very accurate results and in others to conservative responses. One can say this is a safe criterion for designing. In fact, it must not be forgotten that this simplified procedures are developed to be applied in design offices where the results should rather be conservative than almost close to *timehistory* but slightly underestimated.

The results obtained herein seem quite optimistic regarding the implementation of this extended procedure in future codes. Nevertheless, more studies in different buildings should be developed in order to consolidate this nonlinear static approach.

7. CONCLUSIONS

In this endeavour, three real plan-asymmetric RC buildings with three, five and eight storeys were analysed. A comparison between the performance of the CSM-ATC40 and the CSM-FEMA440 recommendations was carried out as a first step of the work. From the obtained results, it was outlined that the features presented in the FEMA440 report led to better results than its predecessor when compared with nonlinear dynamic *timehistory* analyses. For the CM and for the columns located near this node the results obtained with CSM-FEMA440 are close to the *timehistory*, while the ones obtained with the ATC40 are invariantly underestimated. This happens both for the elastic and inelastic range because the ATC40 procedure overestimates the effective damping while the FEMA440 calculates it in a very accurate way. In fact, the innovative methods to compute the effective damping, the demand spectrum reduction factors and the new concept of Modified ADRS introduced in FEMA440 seem to provide more realistic results than the procedure proposed in

DOI: 10.1002/eqe

ATC40. The results of both methods for columns located in the extremities of the buildings were usually not perfectly captured by none of the methods. For this reason an extended version of the CSM-FEMA440 was proposed in the second part of this paper, in order to overcome the torsional problem of plan-asymmetric buildings. This extension was conceived based on the results presented by Fajfar *et al.* and used to extend the N2 method for plan-asymmetric buildings. This extension consists of the application of a correction factor to the pushover results determined by the CSM-FEMA440 recommendations. These correction factors are computed based on a linear RSA and on a pushover analysis. This procedure was evaluated by comparing the results in terms of normalized top displacements with the three case studies and different ground motion intensities. To what torsional effect is concerned it was possible to achieve more realistic and conservative results using the proposed extension than the CSM-FEMA440 original version for all the studied buildings. The proposed extension should be further tested and, if the results came in line with the ones obtained for the three buildings herein studied, it should be incorporated in future codes as a methodology capable of estimating the torsional amplification in plan-asymmetric buildings. The buildings analysed in this study have poor ductility, so the conclusions outlined herein can only be considered for this type of structures. Buildings with higher ductility should be further tested in order to reach definitive conclusions.

ACKNOWLEDGEMENTS

The authors acknowledge the financial support of the Portuguese Foundation for Science and Technology (Ministry of Science and Technology of the Republic of Portugal) through the research project PTDC/ECM/100299/2008 and through the PhD scholarship SFRH/BD/28447/2006 granted to Carlos Bhatt.

REFERENCES

1. Fajfar P, Fischinger M. N2—a method for non-linear seismic analysis of regular buildings. *Proceedings of the Ninth World Conference in Earthquake Engineering*, Tokyo-Kyoto, Japan, vol. 5, 1988; 111–116.
2. Freeman SA. Development and use of capacity spectrum method. *Proceedings of the Sixth U.S. National Conference on Earthquake Engineering*, Seattle, Oakland, U.S.A., 1998.
3. Freeman SA, Nicoletti JP, Tyrell JV. Evaluation of existing buildings for seismic risk—a case study of Puget Sound Naval Shipyard, Bremerton, Washington. *Proceedings of U.S. National Conference on Earthquake Engineering*, Berkeley, U.S.A., 1975; 113–122.
4. Applied Technology Council (ATC). Seismic evaluation and retrofit of concrete buildings, vols. 1 and 2. *Report No. ATC-40*, Redwood City, CA, 1996.
5. Applied Technology Council (ATC). Improvement of nonlinear static seismic analysis procedures. *FEMA 440 Report*, Redwood City, CA, 2005.
6. Chopra AK, Goel RK. A modal pushover analysis procedure to estimate seismic demands for unsymmetric-plan buildings. *Earthquake Engineering and Structural Dynamics* 2004; **33**:903–927.
7. Fajfar P, Marusic D, Perus I. Torsional effects in the pushover-based seismic analysis of buildings. *Journal of Earthquake Engineering* 2005; **9**(6):831–854.
8. Bento R, Bhatt C, Pinho R. Using nonlinear static procedures for seismic assessment of the 3D irregular SPEAR building. *Earthquakes and Structures* 2010; **1**(2):177–195.
9. Fardis MN. Design of an irregular building for the SPEAR Project—description of the 3-storey structure. *Research Report*, University of Patras, Greece, 2002.
10. Fardis MN, Negro P. SPEAR—seismic performance assessment and rehabilitation of existing buildings. *Proceedings of the International Workshop on the SPEAR Project*, Ispra, Italy, 2006.
11. Vuran E, Bal ÝE, Crowley H, Pinho R. Determination of equivalent SDOF characteristics of 3D dual structures. *Proceedings of the 14th World Conference on Earthquake Engineering*, Beijing, China, 2008, paper no: S15-031.
12. SeismoSoft. SeismoStruct—a computer program for static and dynamic nonlinear analysis of framed structures. Available from: www.seismosoft.com, 2006.
13. Mander JB, Priestley MJN, Park R. Theoretical stress–strain model for confined concrete. *ASCE Journal of Structural Engineering* 1988; **114**(8):1804–1826.
14. Martinez-Rueda JE, Elnashai AS. Confined concrete model under cyclic load. *Materials and Structures* 1997; **30**(197):139–147.
15. Menegotto M, Pinto PE. Method of analysis for cyclically loaded RC plane frames including changes in geometry and non-elastic behaviour of elements under combined normal force and bending. *Symposium on the Resistance and Ultimate Deformability of Structures Acted on by Well Defined Loads*, International Association for Bridge and Structural Engineering, Zurich, Switzerland, 1973; 15–22.

DOI: 10.1002/eqe

16. Filippou FC, Popov EP, Bertero VV. Modelling of R/C joints under cyclic excitations. *Journal of Structural Engineering* 1983; **109**(11):2666–2684.
17. CEN. Eurocode 8: design of structures for earthquake resistance. Part 1: general rules, seismic actions and rules for buildings. EN 1998-1:2004 Comité Européen de Normalisation, Brussels, Belgium, 2004.
18. PEER Strong Ground Motion Database. http://peer.berkeley.edu/nga/, 2009.
19. Hancock J, Watson-Lamprey J, Abrahamson NA, Bommer JJ, Markatis A, McCoy E, Mendis R. An improved method of matching response spectra of recorded earthquake ground motion using wavelets. *Journal of Earthquake Engineering* 2006; **10**(S1):67–89.
20. Goel R. Evaluation of current nonlinear static procedures for reinforced concrete buildings. *Proceedings of the 14th World Conference on Earthquake Engineering*, Beijing, China, 2008.

DOI: 10.1002/eqe